Dynamics of optical spin-orbit coupling in uniaxial crystals

Etienne Brasselet,[1,*] Yana Izdebskaya,[2] Vladlen Shvedov,[2,3] Anton S. Desyatnikov,[2] Wieslaw Krolikowski,[2] and Yuri S. Kivshar[2]

[1]*Centre de Physique Moléculaire Optique et Hertzienne, Université Bordeaux 1, CNRS, 33405 Talence Cedex, France*
[2]*Nonlinear Physics Centre and Laser Physics Centre, Research School of Physics and Engineering, The Australian National University, Canberra ACT 0200, Australia*
[3]*Department of Physics, Taurida National University, Simferopol 95007 Crimea, Ukraine*
[*]*Corresponding author: e.brasselet@cpmoh.u-bordeaux1.fr*

Received January 26, 2009; accepted February 12, 2009;
posted February 25, 2009 (Doc. ID 106829); published March 24, 2009

We study theoretically and verify experimentally the detailed dynamics of spin-to-orbital angular momentum conversion for a circularly polarized Gaussian beam propagating along the optical axis of a uniaxial crystal. We extend the results to the case of white-light beams when each of the spectral components undergoes its own wavelength-dependent angular momentum conversion process. © 2009 Optical Society of America

OCIS codes: 260.1180, 260.6042, 350.5500.

Optical angular momentum is a fascinating property of the electromagnetic fields [1]. The light beams can carry spin angular momentum (SAM), associated with their polarization state, and orbital angular momentum (OAM), associated with the spatial structure of the field and phase singularities (or optical vortices) [2,3]. Spin and orbital components of the angular momentum can be separated in isotropic homogeneous media [4] in the limit of paraxial approximation however, they become coupled in inhomogeneous or anisotropic media [5]. Space variant birefringent [6] or form-birefringent [7] elements represent a more complicated class of spin-orbit converters that are simultaneously inhomogeneous and anisotropic. In contrast, spin-to-orbital angular momentum conversion may occur in homogeneous and isotropic media using tightly focused beams, which has been proposed for optical micromanipulation applications [8].

An exchange of the angular momenta between orthogonally polarized beams in anisotropic crystals is of a particular interest [9–16], because the SAM-to-OAM conversion leads to the generation of optical vortices owing to a phase difference between the ordinary and extraordinary waves [9,10,15]. This conversion can be employed as a useful tool for generating polychromatic vortices [15,17], white-light vortex solitons [18], and partially coherent optical bottle beams [19].

In this Letter we study the angular momentum exchanges between the two orthogonal circularly polarized components of Gaussian beams propagating along the optical axis of an uniaxial crystal. Using crystal slabs of different thicknesses we retrieve experimentally the dynamics of optical spin-to-orbital conversion by measuring the power conversion efficiency as well as the beam shape transformations of the coupled singular (double charge optical vortex) and nonsingular (fundamental Gaussian mode) beams. Experimental data are confronted with analytical description of the spin-orbit coupling, and these results are extended to the case of white-light beams, which is spectrally resolved.

First we recall the theory of paraxial beams in uniaxial crystals [9–16]. Modal solution, $\mathbf{E}(x,y,z)=\mathbf{c}^{+}E^{+}(u,v,z)+\mathbf{c}^{-}E^{-}(u,v,z)$, is obtained in the basis of circular polarizations, $\mathbf{c}^{\pm}=(\mathbf{e}_x\pm i\mathbf{e}_y)/\sqrt{2}$, and in terms of the variables $(u,v)=x\pm iy$. It reads $\mathbf{E}^{(s)}=(\mathbf{c}^{+}\partial_u\mp\mathbf{c}^{-}\partial_v)\Phi^{(s)}$, with the generating function satisfying $(i\beta_s\partial_z+\partial_{uv}^2)\Phi^{(s)}=0$. The fundamental Gaussian solution is $\Phi_0^{(s)}=G^{(s)}\equiv-(i\beta_s w^2/Z_s)\exp(i\beta_s uv/Z_s)$, where $Z_s=z-i\beta_s w^2$ and w is the beam waist at the crystal input facet, $z=0$. The signs $\mp$ in the expression for $\mathbf{E}^{(s)}$ correspond to the following values of the index s: $s=o$ for the ordinary (TE) mode with $\beta_o=kn_o/2$, and $s=e$ for the extraordinary (TM) mode with $\beta_e=kn_e^2/2n_o$, $k=2\pi/\lambda$ being the free-space wavenumber.

We are interested in a particular solution that corresponds to a $\mathbf{c}^{+}$ circularly polarized Gaussian beam at the input, $E(r,z=0)=\exp(-r^2/w^2)\mathbf{c}^{+}$. To match these conditions the following superposition of the TE and TM modes is taken $E^{\pm}=\partial_{u,v}(\Phi^{(e)}\pm\Phi^{(o)})$ with generating functions $\Phi^{(s)}=(i/2\beta_s)\int\partial_v G^{(s)}\mathrm{d}z=-(iZ_s/2v\beta_s)G^{(s)}$, or, explicitly,

$$E^{+}=\frac{1}{2}G^{(e)}+\frac{1}{2}G^{(o)}, \tag{1}$$

$$E^{-}=\frac{uv+iZ_e/\beta_e}{2v^2}G^{(e)}-\frac{uv+iZ_o/\beta_o}{2v^2}G^{(o)}. \tag{2}$$

Note that the $\mathbf{c}^{-}$ component E^{-} carries a double-charge vortex and OAM, $E^{-}(r\to0,\varphi,z)\to r^2e^{2i\varphi}w^2(\beta_e^2/Z_e^2-\beta_o^2/Z_o^2)/4$, here $r^2=uv$ and $\varphi=\arg u$. More generally the input Gaussian has an arbitrary polarization, $\mathbf{E}(r,z=0)=(a\mathbf{c}^{+}+b\mathbf{c}^{-})\exp(-r^2/w^2)$, so that the solution above is given by $(a,b)=(1,0)$. In

0146-9592/09/071021-3/$15.00

the opposite case, $(a,b)=(0,1)$, the solution is given for Eqs. (1) and (2) with $E^+ \leftrightarrow E^-$ and $u \leftrightarrow v$. The general solution is obtained by the linear superposition with amplitudes $|a|^2+|b|^2=1$.

To elucidate the coupling between the SAM and OAM for Gaussian beams we note that uniaxial crystals have usually weak birefringence, $n_o-n_e \simeq 10^{-1}-10^{-3}$, so that the anisotropy and its consequence, the spin-orbit coupling, can be considered as a perturbation. Introducing the average refractive index $n=(n_o+n_e)/2$ and the small parameter $\varepsilon=(n_o-n_e)/n \ll 1$ we obtain $\beta_o=\beta(1+\varepsilon/2)$ and $\beta_e \simeq \beta(1-3\varepsilon/2)$, where $\beta=kn/2$, and we keep only the terms of the leading order in ε. Applying such a procedure to Eqs. (1) and (2) we derive the following representation of the general solution, $(E^+,E^-)^T \simeq \hat{\mathbf{M}}(a,b)^T G$, where $G=-(i\beta w^2/Z)\exp(i\beta r^2/Z)$ with $Z=z-iz_0$, $z_0=\beta w^2$, and the transformation matrix

$$\hat{\mathbf{M}} = \begin{pmatrix} C & Se^{-2i\varphi} \\ Se^{2i\varphi} & C \end{pmatrix} = C\hat{\boldsymbol{\sigma}}_0 + S\hat{\mathbf{T}}, \tag{3}$$

$$\hat{\mathbf{T}} = \hat{\boldsymbol{\sigma}}_x \cos(2\varphi) + \hat{\boldsymbol{\sigma}}_y \sin(2\varphi), \tag{4}$$

where $\hat{\boldsymbol{\sigma}}_0$ is identity matrix and $\hat{\boldsymbol{\sigma}}_{x,y}$ are Pauli spinor matrices, $C=\cos\delta$ and $S=-i\sin\delta$ with $\delta=\varepsilon\beta r^2 z/Z^2$. Solution in this form is valid everywhere in the crystal if the anisotropy is small, $\varepsilon \ll 1$.

The matrix representation given by Eqs. (3) and (4) allows one to explore the dynamics of polarization conversion in clear details. Because matrix $\hat{\boldsymbol{\sigma}}_0$ does not change initial polarization state, the first term $C\hat{\boldsymbol{\sigma}}_0$ describes the loss of power of the input beam. In contrast, the second term in Eq. (3), $S\hat{\mathbf{T}}$, shows the power gain experienced by the circularly polarized component that is orthogonal to the initial one and the appearance of OAM compensating the loss of SAM. More precisely, the matrix $\hat{\mathbf{T}}$ changes the handedness of circular polarization and describes the appearance of a vortex with a double topological charge, $|l|=2$, with the sign opposite to the SAM.

Experimentally accessible quantities to retrieve the optical spin-to-orbital conversion are the reduced powers of two components, $P_\pm/P_0=(2/\pi w^2)\int\int|E^\pm|^2 dxdy$, where P_0 is the input power. These quantities are plotted in Fig. 1(a) in the case $(a,b)=(1,0)$ and two different beam waists. Theoretical curves are obtained [9,10] by using Eqs. (1) and (2), $P_\pm/P_0=\frac{1}{2}[1\pm(1+z^2/L^2)^{-1}]$, with $L=2\beta_e\beta_o w^2/(\beta_o-\beta_e)\simeq z_0/\varepsilon$. The angular momenta normalized to the total angular momentum are shown in Fig. 1(b); they are defined as follows: $\mathrm{SAM}_\pm=\pm P_\pm/P_0$ and $\mathrm{OAM}_\pm=l_\pm P_\pm/P_0$ with $l_+=0$ and $l_-=2$.

In our experiments we used uniaxial calcite crystal samples that are cut perpendicularly to the optical axis into 10 mm × 10 mm × z mm slabs for $z=1\ldots14$ mm with steps of 1 mm. Linearly polarized light from a He–Ne laser operating at wavelength $\lambda=633$ nm ($n_o=1.656$ and $n_e=1.458$) is converted into circular polarization using a quarter-wave plate. The beam is then focused by a lens ($f=25$ mm) onto the sample whose optical axis coincides with the direction of propagation. The output beam is collimated by a second lens ($f=100$ mm) and passes through a second quarter-wave plate and a polarizing beamsplitter, which allows us to separate its orthogonally polarized double-charge optical vortex and fundamental Gaussian components.

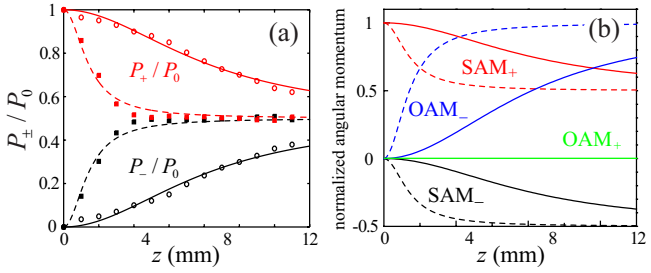

Fig. 1. (Color online) Transfer of normalized (a) powers and (b) angular momenta between $\mathbf{c}^+$ (red, green, plus) and $\mathbf{c}^-$ (black, blue, minus) circularly polarized components. Curves, theory; markers, experiment. The beam waist $w=4.59$ μm (squares, dashed curves) and $w=11.02$ μm (circles, solid curves).

The intensity distributions of the $\mathbf{c}^+$ ($l=0$) and $\mathbf{c}^-$ ($l=2$) circularly polarized components of a monochromatic beam are shown in Fig. 2 for various propagation distances z. Both circular components exhibit

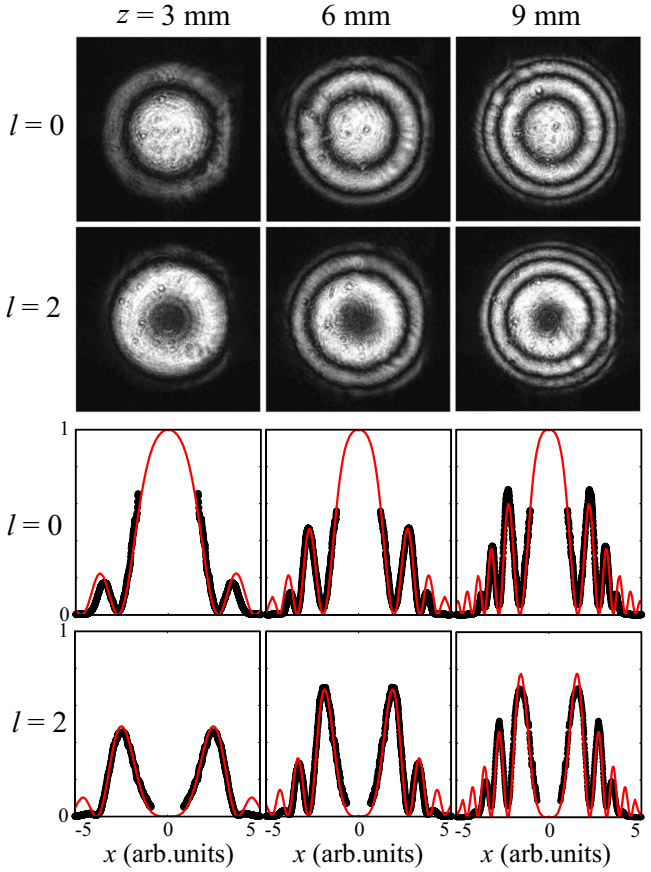

Fig. 2. (Color online) Experimentally measured intensity profiles for two components $|E^\pm|^2$ of the laser beam with $\lambda=633$ nm and $w=4.59$ μm. The thin (red) curves in the bottom diagrams were calculated using Eqs. (1) and (2), and the thick (black) curves are obtained by averaging the experimental ring profiles over azimuth.

annular profiles while spreading during propagation, which correspond to dislocation rings. Dark spots can be observed at the center of the images for $l=2$. These spots support the evidence of the phase singularity in the center of the helical beam, which is confirmed by the charge two singular interference pattern when the beam is superimposed with the fundamental Gaussian beam (not shown). We also compare in Fig. 2 the measured and calculated radial intensity profiles of the beams. The dislocation rings, the power reduction–rise of the $\mathbf{c}^{\pm}$ components are all reproduced quantitatively with a good agreement.

Analogous experiments were performed using a circularly polarized white-light input quasi-Gaussian beam derived from a halogen lamp with a power of 50 W and angular divergence 8°. Light from the lamp passes first through the bundle of optical fibers (with an aperture of 5 mm) and then through an IR filter that limits the spectral range to 440–800 nm. The beam is then collimated by a microscope objective and an aperture thereby attaining a nearly Gaussian intensity profile. After the aperture, the light passes through a polarizer and an achromatic quarter-wave plate, thus acquiring circular polarization. Other details of the setup are the same as for monochromatic light.

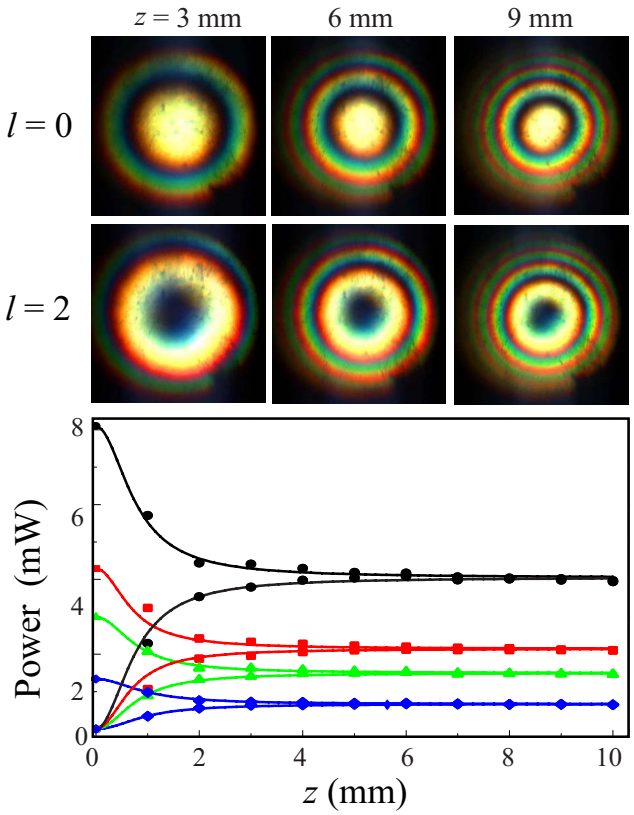

Fig. 3. (Color online) Intensity profiles of the circularly polarized components (E^{+}, top row; E^{-}, bottom row) of a white-light beam at the output of calcite slabs with different thicknesses. Bottom diagram: power of three main spectral components versus z for $w=4.33$ μm. Solid curves, markers: theory, experiment. Blue, diamonds: $\lambda=440$ nm; green, triangles: $\lambda=550$ nm; red, squares: $\lambda=630$ nm; and black, circles: total white light with mean wavelength $\bar{\lambda}=0.573$ μm and spectral width $\Delta\lambda\simeq 0.36$ μm.

Figure 3 shows the intensity distribution (top) and the power dynamics (bottom) of the polarization conversion for a white-light beam. The powers of the main spectral components are obtained using colored glass filters. The power dynamics of each spectral component follows the analytical formula but with its own parameter $L(\lambda)$. Using known data for the dispersion of calcite crystals, we find $L\simeq 1.75$ mm for blue, 1.44 mm for green, and 1.28 mm for red light. The corresponding predicted powers shown in Fig. 3 solid curves) demonstrate a good agreement with experimental data (circles).

In conclusion, we have studied theoretically and experimentally the dynamics of optical spin-to-orbital angular momentum conversion using circularly polarized Gaussian beams propagating along the optical axis of perpendicularly cut uniaxial crystal slabs. Theory well describes experimental observations for both monochromatic and polychromatic light beams.

We thank A. Volyar for useful discussions and acknowledge the Australian Research Council for partial financial support.

References

1. L. Allen, S. M. Barnet, and M. J. Padgett, *Optical Angular Momentum* (IoP, 2003).
2. L. Allen, M. W. Beijersbergen, R. J. C. Spreeuw, and J. P. Woerdman, Phys. Rev. A **45**, 8185 (1992).
3. M. Vasnetsov and K. Staliunas, *Optical Vortices*, Vol. 228 of Horizons of World Physics (Nova Science, 1999).
4. N. B. Simpson, K. Dholakia, L. Allen, and M. J. Padgett, Opt. Lett. **22**, 52 (1997).
5. V. Liberman and B. Zeldovich, Phys. Rev. A **46**, 5199 (1992).
6. L. Marrucci, C. Manzo, and D. Paparo, Phys. Rev. Lett. **96**, 163905 (2006).
7. G. M. Lerman and U. Levy, Opt. Lett. **33**, 2782 (2008).
8. Y. Zhao, J. S. Edgar, G. D. M. Jeffries, D. McGloin, and D. T. Chiu, Phys. Rev. Lett. **99**, 073901 (2007).
9. A. Ciattoni, G. Cincotti, and C. Palma, J. Opt. Soc. Am. A **20**, 163 (2003).
10. A. Ciattoni, G. Cincotti, and C. Palma, Phys. Rev. E **67**, 036618 (2003).
11. N. S. Kasak, N. A. Khio, and A. A. Ryzhevich, Quantum Electron. **29**, 1020 (1999).
12. M. Berry and M. Dennis, Proc. R. Soc. London Ser. A **459**, 1261 (2003).
13. A. Volyar and T. Fadeyeva, Opt. Spectrosc. **94**, 264 (2003).
14. A. Volyar and T. Fadeyeva, Opt. Spectrosc. **101**, 297 (2006).
15. Yu. Egorov, T. Fadeyeva, and A. Volyar, J. Opt. A **6**, S217 (2004).
16. F. Flossmann, U. Schwarz, M. Maier, and M. Dennis, Opt. Express **14**, 11402 (2006).
17. A. Volyar, V. Shvedov, T. Fadeyeva, A. S. Desyatnikov, D. N. Neshev, W. Krolikowski, and Yu. S. Kivshar, Opt. Express **14**, 3724 (2006).
18. D. N. Neshev, A. Dreischuh, V. Shvedov, A. S. Desyatnikov, W. Krolikowski, and Yu. S. Kivshar, Opt. Lett. **33**, 1851 (2008).
19. V. Shvedov, Ya. V. Izdebskaya, A. V. Rode, A. S. Desyatnikov, W. Krolikowski, and Yu. S. Kivshar, Opt. Express **16**, 20902 (2008).